analytical chemistry

Article

Cite This: *Anal. Chem.* 2018, 90, 9983−9989

pubs.acs.org/ac

2D-Metal−Organic-Framework-Nanozyme Sensor Arrays for Probing Phosphates and Their Enzymatic Hydrolysis

Li Qin,[†,§] Xiaoyu Wang,[†,§] Yufeng Liu,[†] and Hui Wei*[,†,‡]

[†]Department of Biomedical Engineering, College of Engineering and Applied Sciences, Nanjing National Laboratory of Microstructures, Nanjing University, Nanjing, Jiangsu 210093, China

[‡]State Key Laboratory of Analytical Chemistry for Life Science and State Key Laboratory of Coordination Chemistry, School of Chemistry and Chemical Engineering, Collaborative Innovation Center of Chemistry for Life Sciences, Nanjing University, Nanjing, Jiangsu 210023, China

Supporting Information

ABSTRACT: The detection of phosphates and their enzymatic hydrolysis is of great importance because of their essential roles in various biological processes and numerous diseases. Compared with individual sensors for detecting one given phosphate at a time, sensor arrays are able to discriminate multiple phosphates simultaneously. Although nanomaterial-based sensor arrays have shown great promise for the discrimination of phosphates, very few of them have been explored for probing phosphates involved enzymatic hydrolysis. To fill this gap, herein we fabricated two-dimensional-metal−organic-framework (2D-MOF)-nanozyme-based sensor arrays by modulating their peroxidase-mimicking activity with various phosphates, including AMP, ADP, ATP, pyrophosphate (PPi), and phosphate (Pi). The sensor arrays were used to successfully discriminate the five phosphates not only in aqueous solutions but also in biological samples. The practical application of the sensor arrays was then validated with blind samples, where 30 unknown samples containing phosphates were accurately identified. Moreover, the sensor arrays were successfully applied to probing hydrolytic processes involving ATP and PPi that are catalyzed by apyrase and PPase, respectively. This work demonstrates a nanozyme-based sensor array as a convenient and reliable analytical platform for probing phosphates and their related enzymatic processes, which could be applied to other analytes and enzymatic reactions.

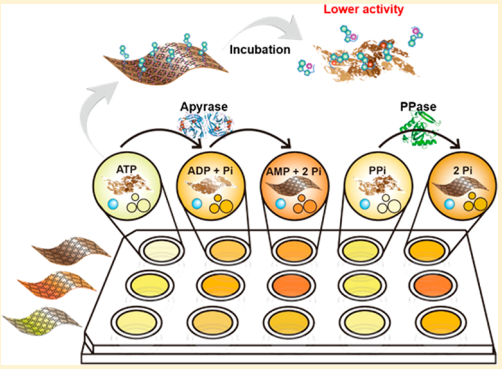

Phosphates have diverse forms, including AMP, ADP, ATP, pyrophosphate (PPi), and phosphate (Pi), all of which play essential roles in various biological processes, such as cellular signaling and energy metabolism.[1,2] In particular, different phosphates can be catalytically interconverted by their corresponding enzymes. These enzymatic interconversions are fundamental in cellular events and are directly related to metabolism and numerous diseases.[3] For instance, the hydrolysis of ATP by ATPase supplies energy to organisms, and the dysregulation of this hydrolysis can lead to hypoglycemia, ischemia, and circulatory shock.[4,5] The decomposition of PPi by PPase is closely associated with lipid metabolism and calcium absorption.[6] In order to elucidate the roles of phosphates in related physiological and pathological events, it is necessary not only to detect the particular substrates (*e.g.*, ATP and PPi) and hydrolysates (*e.g.*, AMP and Pi) simultaneously but also to follow the whole enzymatic processes.

In recent years, plenty of sensing systems for phosphates have been established, including fluorescent,[7,8] colorimetric,[9,10] and electrochemical sensors.[11,12] These individual sensors, however, were usually designed for detecting one given phosphate at a time. Sensor arrays have therefore been extensively studied to discriminate multiple phosphates simultaneously. Regarded as artificial noses and tongues, sensor arrays consisting of multiple channel-sensing elements can give cross-reactive signals to each analyte without the problem of selectivity.[13−19] More encouragingly, sensor arrays have even been used for tracking patterns to follow real-time biologically related events.[18,20] Up to now, various sensing elements, such as fluorescent dyes and chromogenic polymers, have been used to construct sensor arrays for phosphates.[21,22] However, these organic materials are complicated to synthesize, and their signals are sensitive to reaction conditions, imposing restrictions on their practical applications. To this end, functional nanomaterials with facile synthesis and high robustness have recently been employed to develop sensor arrays for phosphates. For example, fluorescent carbon dots were utilized to fabricate a sensor array for the discrimination of phosphates.[23] Despite the exciting success of functional-nanomaterial-based sensor arrays, very few of them have been explored for probing enzymatic

Received: May 31, 2018
Accepted: July 25, 2018
Published: July 25, 2018

DOI: 10.1021/acs.analchem.8b02428
Anal. Chem. 2018, 90, 9983−9989

processes, especially hydrolysis involving phosphates. To fill this gap, herein we fabricated two-dimensional-metal−organic-framework (2D-MOF)-nanozyme-based sensor arrays and used them for discriminating phosphates as well as for following phosphate-related enzymatic hydrolysis.

Nanozymes are functional nanomaterials with emerging enzyme-like activities.[24−31] Because of their much more stable catalytic activities and lower cost compared with those of natural enzymes, they have recently been developed for wide applications, including biosensing.[32−40] A few pioneering studies have shown that the nanozyme sensor arrays composed of gold or iron oxide nanoparticles could be used for protein discrimination.[41−43] Inspired by these, we envisaged that 2D-MOF nanozymes are good alternatives to gold or iron oxide nanoparticles for sensor arrays because of their tailorable structures and catalytic activities as well as their highly exposed surfaces and active sites.[44] In this work, we demonstrated that the peroxidase-mimicking activities of a series of 2D-MOF nanozymes could be modulated by various phosphates, forming the basis of the designed sensor arrays for phosphate discrimination. The sensor arrays were used to discriminate phosphates (Figure S1), even in biological samples and in blind samples. More importantly, two representative hydrolytic processes, ATP and PPi catalyzed by apyrase and PPase, were successfully followed with the designed 2D-MOF-nanozyme sensor arrays (Scheme 1).

Scheme 1. Schematic of 2D-MOF-Nanozyme Sensor Arrays Probing Phosphates and Their Related Hydrolytic Processes

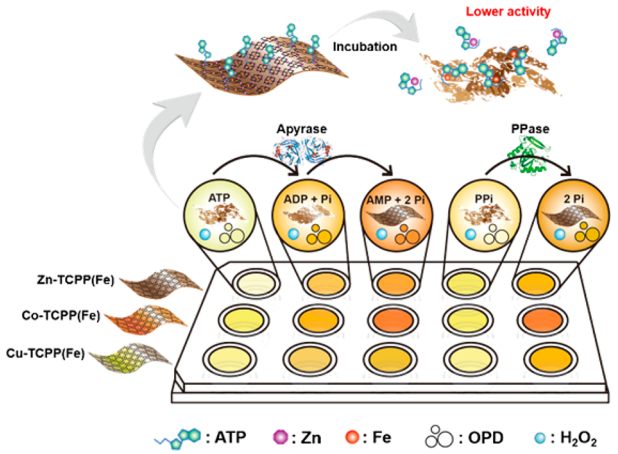

EXPERIMENTAL SECTION

Reagents and Materials. All reagents were at least analytical grade. Zinc nitrate hexahydrate ($Zn(NO_3)\cdot 6H_2O$), cobalt nitrate hexahydrate ($Co(NO_3)_2\cdot 6H_2O$), copper nitrate hydrate ($Cu(NO_3)_2\cdot 3H_2O$), adenosine 5′-triphosphate disodium salt (ATP), adenosine 5′-diphosphate sodium salt (ADP), ammonium molybdate tetrahydrate, hydroquinone, 3,3′,5,5′-tetramethylbenzidine dihydrochloride (TMB), and 2,2′-azinobis(3-ethyl benzothiazoline-6-sulfonic acid) ammonium (ABTS) were purchased from Aladdin Chemical Company Ltd. Polyvinylpyrrolidone (PVP, MW 40 000) and adenosine 5′-monophosphate sodium (AMP) were purchased from Sigma-Aldrich. Fe(III) tetra(4-carboxyphenyl)porphyrin chloride (TCPP(Fe)) was purchased from J&K Scientific Company Ltd. Sodium pyrophosphate (PPi) was purchased from Kermel Reagent. *N*,*N*-Dimethylformamide (DMF), dimethyl sulfoxide (DMSO), sodium phosphate tribasic dodecahydrate ($Na_3PO_4\cdot 12H_2O$, Pi), potassium phosphate monobasic (KH_2PO_4), sodium sulfite (Na_2SO_3), potassium persulfate ($K_2S_2O_8$), hydrogen peroxide (H_2O_2), *o*-phenylenediamine (OPD), and sodium acetate trihydrate (NaOAc) were purchased from Sinopharm Chemical Reagent Company Ltd. All aqueous solutions were prepared with deionized water (18.2 MΩ·cm, Millipore).

Synthesis of 2D M-TCPP(Fe) Nanozymes (M = Zn, Co, or Cu). The three nanozymes were prepared according to our previous method.[45]

Peroxidase-Mimicking-Activity Measurements. The peroxidase-mimicking activity of the 2D-MOF nanozymes was evaluated by using the peroxidase chromogenic substrates (TMB, OPD, and ABTS). Briefly, 10 μL of a 2D-MOF DMSO suspension (100 μg/mL) was added into 0.2 M acetate buffer (pH 4.5) containing H_2O_2 (50 mM) and a chromogenic substrate (1 mM TMB, 1 mM ABTS, or 2 mM OPD). The final volume of the mixture was adjusted to 1 mL with 0.2 M acetate buffer (pH 4.5). The mixed solution was then incubated at room temperature for 1 min. Then, the resulting reaction solution was used for absorption-spectroscopic measurements on a UV−vis spectrophotometer.

Effect of Phosphates on 2D-MOF-Nanozyme Activity. To study the effects of phosphates on the activity of the nanozymes, mixtures of 2D-MOF nanozymes (2 μg) and different amounts of phosphates were incubated in NaOAc buffer (0.2 M, pH 4.5) for 20 min. Then, 100 μL of H_2O_2 (1 M) and 100 μL of OPD (20 mM) were added to a final volume of 1 mL. After further incubation at room temperature for 15 min, the absorption spectra were measured on a UV−vis spectrophotometer.

Procedures for the Discrimination of Phosphates Based on Sensor Arrays. In a 96-well plate, a 6 × 6 region was selected in which the blank and five kinds of phosphates (AMP, ADP, ATP, PPi, and Pi) occupied a 6-well row. Buffer solution (80 μL, 0.2 M NaOAc, pH 4.5) that included the appropriate amounts of phosphates and 2D-MOF nanozymes was added into each well. After incubation for 10 min at room temperature, 10 μL of H_2O_2 (1 M) and 10 μL of OPD (20 mM) were rapidly added into each well sequentially to a final volume of 100 μL. Immediately after the addition of the chromogenic substrate, the absorption of each well at 450 nm was recorded by a microplate reader at intervals of 5 min for 30 min. The concentration of 2D-MOF nanozymes was 2 μg/mL. As a consequence, the 5 kinds of phosphates were tested against the 3 kinds of 2D-MOF nanozymes 6 times each to give a training-data matrix of 5 phosphates × 3 arrays × 6 replicates. The data were processed by linear discriminant analysis.

Probing ATP- and PPi-Involved Hydrolytic Processes and Their Metabolites. ATP can be hydrolyzed into ADP, AMP, and Pi in the presence of ATPase. Apyrase (ATPase/ADPase = 1:1, termed as apyrase (1:1)) is a typical example; 1 mM ATP and 0.48 U/mL apyrase (1:1) were mixed in 2.0 mM Tris-HCl buffer (pH 7.4) containing 0.08 mM EDTA, 0.7 mM $MgCl_2$, 3.4 mM NaCl, and 0.07 mM KCl at 37 °C. The final volume of mixture solution was 1.5 mL, and the hydrolysis-assay samples were collected at different hydrolysis intervals (0, 10, 20, and 30 min). After centrifugation and dilution, the assay samples of 100 μM were analyzed at different time points with control samples in sensor arrays to obtain a training data

DOI: 10.1021/acs.analchem.8b02428
Anal. Chem. 2018, 90, 9983−9989

matrix. Apyrase (ATPase/ADPase = 10:1, termed as apyrase (10:1))- and PPase-catalyzed reaction processes and their metabolites were analyzed by sensor arrays with similar procedures as well. The data matrices were also processed by linear discriminant analysis.

Total Phosphorus Quantification by a Molybdenum-Blue Colorimetric Method. All the samples in the colorimetric method were diluted to the appropriate concentrations and divided into 1.5 mL aliquots. Then, 1 mL of 25 mg/mL ammonium molybdate, 0.5 mL of 5 mg/mL hydroquinone, and 0.5 mL of 200 mg/mL Na_2SO_3 were added to each sample separately. Thirty minutes after being mixed, the resulting reaction solution was used for absorption spectroscopy on a UV−vis spectrophotometer. In a typical digestion procedure, a moderate amount of sample was digested by $K_2S_2O_8$ in acidic conditions. In short, 0.6 mL of 0.5 M H_2SO_4 and 2.4 mL of a $K_2S_2O_8$ solution were added to the sample solution, and the final volume of the mixture was adjusted to 9 mL with water. After being mixed for a while, the reaction solution was transferred to a 20 mL autoclave and heated to 120 °C for 2 h in a drying oven. All the organophosphorus was digested into orthophosphate and quantified via the molybdenum-blue colorimetric method after digestion.[46]

Instrumentation. TEM images were recorded on a JEOL JEM-2100 transmission electron microscope at an acceleration voltage of 200 kV. The diffractometer was operated at 40 kV and 40 mA with a scan rate of 2°/min. UV−vis absorption spectra were recorded on a UV−vis spectrophotometer (Cary-100, Agilent Technologies). The absorption of the 96-well plates at 450 nm was recorded by a microplate reader (RT-6000, Rayto Life and Analytical Sciences Company, Ltd.). DLS characterization was performed on a Zetasizer Nano ZS 90 (Malvern).

RESULTS AND DISCUSSION

Modulation of Peroxidase-Mimicking Activity of 2D-MOF Nanozymes by Phosphates. Recently, we reported the synthesis of 2D-MOF nanozymes consisting of three kinds of divalent metal ions (*i.e.*, Zn^{2+}, Co^{2+}, and Cu^{2+}) and a heme-like metalloporphyrin ligand (*i.e.*, TCPP(Fe)).[45] They were termed 2D Zn-TCPP(Fe), 2D Co-TCPP(Fe), and 2D Cu-TCPP(Fe), respectively (Figure S2). We studied their peroxidase-mimicking activities, which were further confirmed in the current study using three classical chromogenic substrates (*i.e.*, TMB, OPD, and ABTS; Figures S3 and S4). We showed that TCPP(Fe) is the main active site of the 2D-MOF nanozymes, whereas the divalent metal ions act as the junction sites. Because the current sensor arrays were based on the modulation of peroxidase-mimicking activity of the three 2D-MOF nanozymes, we first investigated the effects of different phosphates on the nanozymes' activities. Taking 2D Zn-TCPP(Fe) as an example, different amounts of ATP were added into the catalytic-oxidation-reaction solution containing H_2O_2 and OPD. The typical absorption spectra around 450 nm are displayed in Figure 1a, illustrating the dose-dependent inhibitory ability of ATP on the peroxidase-mimicking activity of 2D Zn-TCPP(Fe). Similarly, the inhibition capacities of other phosphates were also investigated (Figure S5). As summarized in Figure 1b, ATP and PPi strongly inhibited the activity, whereas AMP and Pi were much weaker at the same concentration. For 2D Co-TCPP(Fe) and 2D Cu-TCPP(Fe), similar modulation effects of the phosphates on 2D Zn-TCPP(Fe) were observed (Figures S6 and S7). As the binding between junction metal ions and phosphates is stronger than that between junction metal ions and the carboxyl groups of TCPP(Fe),[47,48] the addition of phosphates deprives the junction ions of 2D-MOF nanosheets, triggering the collapse of the whole 2D structure and damping the mimicking activity. To verify this hypothesis, a mixture of Zn-TCPP(Fe) nanosheets and the appropriate amount of ATP was characterized by TEM after incubation. As shown in Figure 1c, the fragmentary Zn-TCPP(Fe) indicated that the integrated 2D structure had collapsed after the addition of ATP, which was further evidenced by dynamic-light-scattering (DLS) measurements (Figure S8). To further understand the inhibitory effects of the phosphates, we studied the peroxidase-like activity of the TCPP(Fe) monomer (*i.e.*, the active site of the 2D-MOF nanozymes) in the presence of the phosphates. As shown in Figure 1d, the five phosphates had different inhibitory effects on the activity of TCPP(Fe), which could be attributed to the different interactions of the phosphates with the Fe atom in TCCP(Fe).[49] The whole reaction process can be summarized as follows. The interaction between phosphates and junction ions triggers the collapse of the 2D structure, which in turn promotes the interaction between the phosphates and the TCPP(Fe) monomer, resulting in the inhibition of the nanozymes' mimicking activity. Moreover, the five phosphates exhibited different affinities with the same metal nodes, and each phosphate also showed different binding abilities with different metal nodes, leading to three signal channels for constructing the sensor array.

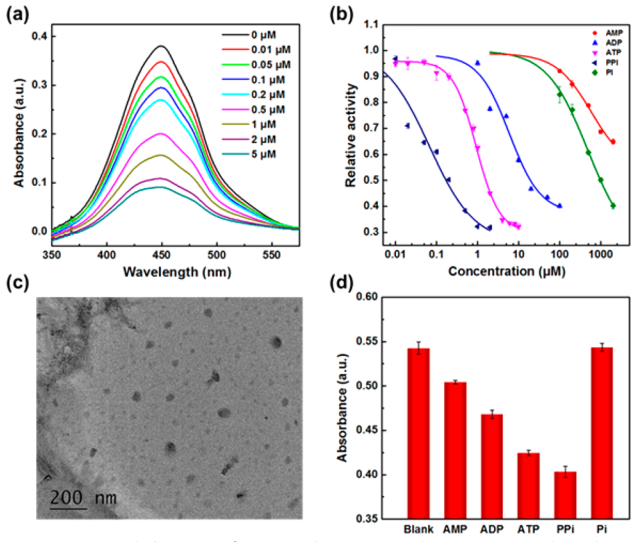

Figure 1. Modulation of peroxidase-mimicking activity by phosphates. (a) Typical absorption spectra for monitoring the catalytic oxidation of OPD in the presence of Zn-TCPP(Fe) nanosheets with various concentrations of ATP. (b) Normalized peroxidase-mimicking activity of Zn-TCPP(Fe) nanosheets after incubation with different concentrations of the five phosphates. Each error bar shows the standard deviation of four independent measurements. (c) TEM image of Zn-TCPP(Fe) nanosheets after incubation with 10 μM ATP for 20 min. (d) Peroxidase-mimicking activity (absorbance at 450 nm) of TCPP(Fe) after incubation with the five phosphates. The concentrations of TCPP(Fe) and the phosphates were 2 μg/mL and 10 μM, respectively. Each error bar shows the standard deviation of six independent measurements.

Discrimination of Phosphates by Sensor Arrays. Because the different phosphates had such distinct diversity

DOI: 10.1021/acs.analchem.8b02428
Anal. Chem. 2018, 90, 9983−9989

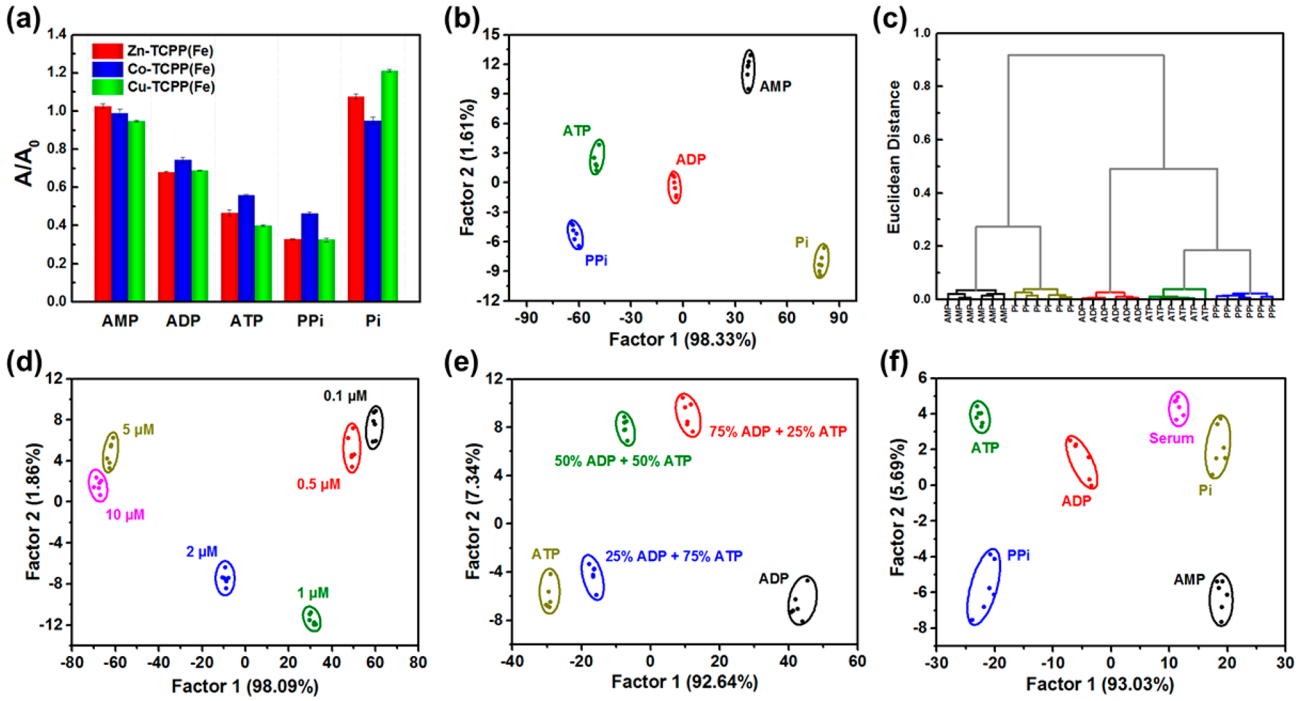

Figure 2. Sensor arrays for phosphates. (a) Colorimetric-response patterns (A/A_0) of nanozyme sensor arrays toward 10 μM phosphates. Each error bar shows the standard deviation of six independent measurements. (b) 2D canonical score plot for the first two factors of the colorimetric-response patterns obtained against 10 μM phosphates. (c) Hierarchical-cluster-analysis (HCA) plot for the discrimination of phosphates generated from the colorimetric-response patterns toward 10 μM phosphates. (d–f) 2D canonical score plots for the first two factors of the colorimetric-response patterns obtained against different concentrations of ATP (d), mixtures of phosphates with different molar ratios and total concentrations of 5 μM (e), and 10 μM phosphates in the presence of 0.1% FBS (f). The canonical scores were calculated by LDA for the identification and discrimination of phosphates.

in terms of inhibition of the peroxidase-mimicking activity of the 2D-MOF nanozymes, colorimetric-method-based sensor arrays for phosphates were established. Phosphates of the same concentration (10 μM) were incubated with the three nanozymes and OPD (as the chromogenic substrate) for a period of time in the presence of H_2O_2. We employed the parameter A/A_0 to describe the inhibitory capacity of each phosphate, where A was the absorbance of oxidized OPD (oxOPD) at 450 nm in the presence of phosphates, and A_0 was that of the blank one without phosphates. As shown in Figure 2a, the catalytic oxidation of OPD with the nanozymes was modulated to varying degrees in the presence of different phosphates. We could not intuitively discriminate the results on the basis of the data points in 3D space (Figure S9); therefore, linear discriminant analysis (LDA) was used to convert the training matrix (3 MOF nanozymes × 5 phosphates × 6 replicates) into three canonical scores (similar to projection), and the first two most significant discrimination factors (98.33% and 1.61%) were used to generate a 2D canonical score plot (Figure 2b). In a hierarchical-cluster-analysis (HCA) pattern (Figure 2c), five different phosphates could also be clearly distinguished without cross influences. Thus, a sensor array consisting of three kinds of 2D-MOF nanozymes was fabricated that could efficiently discriminate the five phosphates from 2 to 500 μM (Figures S10–S14), demonstrating great differentiation capacity in an extensive concentration range.

Practical Applications of Nanozyme Sensor Arrays. On the basis of discrimination results obtained, we then applied the sensor arrays to more practical areas. To demonstrate the quantification function of the sensor arrays, we first tested the discrimination capability of the sensor arrays toward various concentrations of ATP. ATP was chosen as the model analyte because it is the most significant phosphate related to energy-supply reactions in cells. Different concentrations of ATP ranging from 0.1 to 10 μM were clearly distinguished in the LDA patterns (Figures 2d and S15a). Furthermore, there was a good linear relationship between Factor 1 of each cluster in the pattern and the ATP concentration from 0.1 to 2 μM (Figure S16), which could be used to quantify the concentration. To assess the applicability of the sensor array to discriminate coexisting phosphates, mixtures of ATP and ADP with different molar ratios (ATP/ADP = 75:25, 50:50, and 25:75 at a total concentration of 5 μM) were investigated. ADP was adopted here because it is another essential phosphate in bioenergetics and often coexists with ATP. As shown in Figures 2e and S15b, the mixtures of ATP and ADP, as well as the solutions of pure ATP and ADP, were clearly distinguished from each other in the LDA patterns. Furthermore, we investigated the discrimination ability of the sensor arrays in biological samples because the concentrations of phosphates in serum are important indicators in clinical diagnostics. Clear discrimination of different phosphates at a relatively low concentration (10 μM) in 0.1% FBS (Figures 2f and S15c), as well as at 50 μM in 1% FBS (Figure S17), was achieved.

The next challenge lays in discriminating blind samples of unknown concentrations. Because the discrimination principle of sensor arrays depended on the concentrations of phosphates in the samples, the LDA patterns at different concentrations were totally different. To discriminate blind samples containing phosphates, it is necessary to determine the total amount of

DOI: 10.1021/acs.analchem.8b02428
Anal. Chem. 2018, 90, 9983–9989

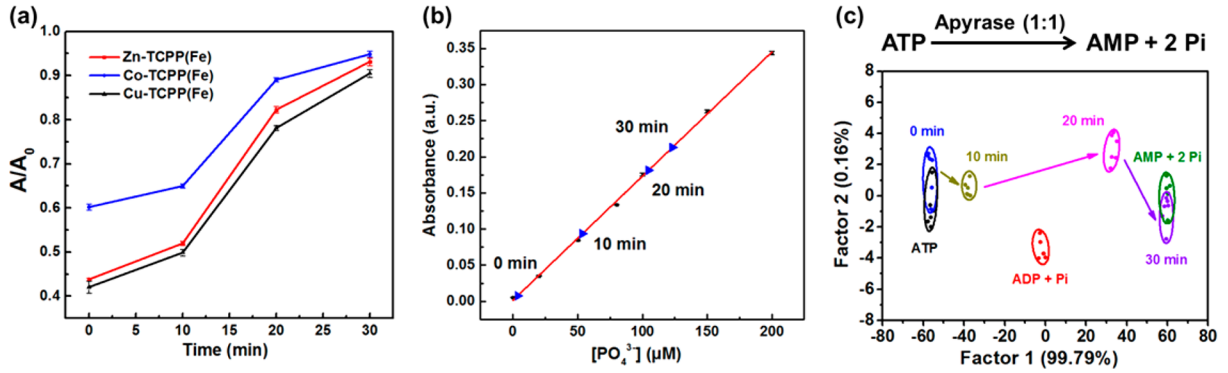

Figure 3. Probing apyrase (1:1)-catalyzed hydrolytic reactions by sensor arrays. (a) A/A_0 responses of the hydrolytic process catalyzed by apyrase (1:1) over time. Each error bar shows the standard deviation of six independent measurements. (b) Molybdenum-blue-colorimetric-method quantification of hydrolysates catalyzed by apyrase (1:1) over time. All assay samples (100 μM) were further diluted 1.5 times. (c) 2D canonical score plot for the first two factors of response patterns obtained against ATP, ADP + Pi, AMP + 2Pi, and assay samples from different time points in the ATP-hydrolysis process catalyzed by apyrase (1:1). The concentrations of the control and assay samples were 10 μM.

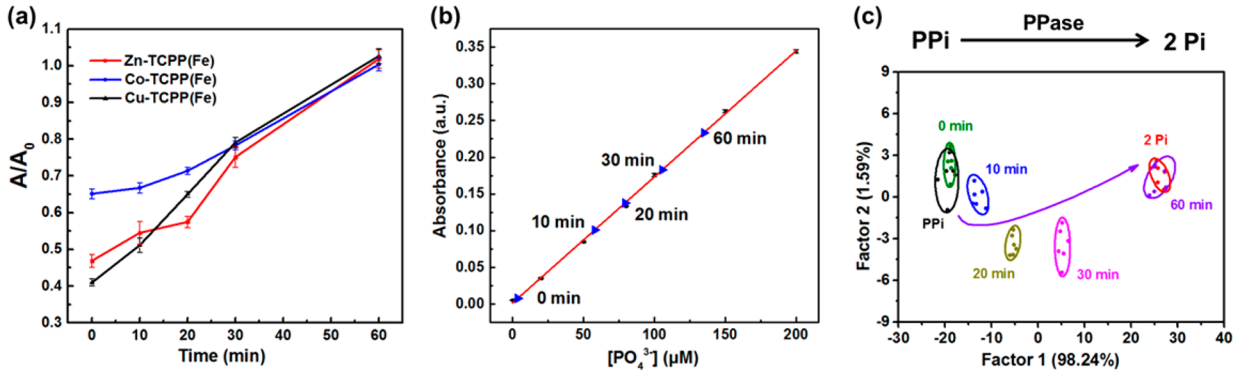

Figure 4. Probing PPase-catalyzed hydrolytic reactions by sensor arrays. (a) A/A_0 responses of the hydrolytic process catalyzed by PPase over time. Each error bar shows the standard deviation of six independent measurements. (b) Molybdenum-blue-colorimetric-method quantification of hydrolysates catalyzed by PPase. All assay samples (100 μM) were further diluted 1.5 times. (c) 2D canonical score plot for the first two factors of response patterns obtained against PPi, 2Pi, and assay samples from different time points in the PPi-hydrolysis process catalyzed by PPase. The concentrations of the control and assay samples were 1 μM. The canonical scores were calculated by LDA for the identification and discrimination of phosphates in catalytic reactions.

phosphates first. The molybdenum-blue colorimetric method, a well-established method for the determination of total phosphorus concentrations, was employed to quantify the blind samples (Figure S18).[50,51] The blind samples were then diluted to a given total phosphorus concentration after quantification. By comparing the canonical score plot of training data with the phosphates in the testing data at the same total phosphorus concentration (*e.g.*, 30 μM), blind samples were quantitatively and qualitatively analyzed. The identification of 30 blind samples achieved 100% accuracy (Figure S19 and Table S1).

Probing ATP- and PPi-Involved Hydrolytic Processes and Their Metabolites. Because the proposed sensor arrays had an excellent phosphate identification capacity, we applied them to monitor hydrolytic reactions catalyzed by two important hydrolases: apyrase and PPase. Hydrolysis reactions involving ATP and PPi are among the most essential processes related to energy supply and metabolism. The enzymes catalyze the hydrolysis of the ester bonds in ATP and PPi, leading to the breakage of the phosphoester bond and the release of high energy. We first examined the theoretical hydrolysates of 10 μM ATP and PPi, proving the feasibility that the sensor arrays could effectively distinguish these metabolites at a relatively low concentrations (Figure S20). Practically, apyrase has two isoenzymes, the difference lies on the ratio of its ATPase and ADPase, and it can differ as a result of the ratio of these two enzymes. Taking apyrase with ATPase/ADPase = 1:1 (apyrase (1:1)) as an example, ATP will first be hydrolyzed into ADP and Pi in the presence of ATPase, and then ADPase catalysis will result in AMP with two Pi. The appropriate amount of ATP and apyrase (1:1) were mixed and reacted under optimal conditions (in a biomimetic buffer and at a suitable temperature). After centrifugation and dilution, the assay samples at different time points were analyzed by sensor arrays. As the hydrolysis reaction proceeded, the values of A/A_0 increased because of the much weaker inhibition of the peroxidase-mimicking activity of 2D-MOF nanozymes by AMP and Pi compared with that by ATP, indicating the hydrolysis of ATP (Figures 3a and S21a). The hydrolytic process was confirmed by the molybdenum-blue colorimetric method (Figure 3b). At time 0 min, nearly no Pi could be detected, and more Pi could be probed over time. After 30 min, almost all the ATP had been converted into AMP and Pi, corresponding to the reaction equation. The A/A_0 responses terminated at various time points were subjected to LDA, together with those of the control samples. As illustrated in Figure 3c, under the catalysis of apyrase (1:1) over 30 min, the point cluster of 0 min

DOI: 10.1021/acs.analchem.8b02428
Anal. Chem. 2018, 90, 9983−9989

coinciding with ATP gradually approached and finally coincided with the cluster of AMP with two Pi. The analysis not only showed the whole catalytic process in the fingerprint pattern but also determined the state of the mixture when combined with the molybdenum-blue colorimetric method. Similarly, we obtained the corresponding data matrices of the hydrolytic processes of ATP catalyzed by apyrase (10:1) in Figure S22.

To demonstrate the generality of the sensor array for probing phosphates involved in hydrolysis, the PPi-hydrolysis process catalyzed by PPase was investigated. Figures 4a,b and S21b show the A/A_0 responses and colorimetric results of the whole PPi-hydrolysis process catalyzed by PPase. After 60 min, PPi was completely converted into Pi as evidenced by the fingerprint pattern (Figure 4c). As the PPase-catalyzed hydrolysis reaction proceeded, the point cluster of assay samples generated from different time points moved from the position of PPi to the position where two Pi was located, displaying the whole hydrolytic process in the LDA pattern.

CONCLUSIONS

In summary, we established 2D-MOF-nanozyme sensor arrays to distinguish different phosphates and to probe the related enzymatic-hydrolysis processes. On the basis of the effective modulation of the peroxidase-mimicking activity of 2D-MOFs by phosphates, the developed sensor arrays showed great discrimination ability toward five biologically important phosphates. The fabricated sensor arrays were successfully applied to the detection of phosphates both in aqueous solutions and in biological samples. Moreover, the blind samples of unknown concentrations were accurately identified by combining the sensor arrays with a molybdenum-blue colorimetric method. Most notably, the ATP- and PPi-related enzymatic-hydrolysis processes were clearly monitored with the sensor arrays. This study not only provides a convenient tool to probe phosphates and their related enzymatic processes, but it also broadens the applications of nanozymes and sensor arrays.

ASSOCIATED CONTENT

Supporting Information

The Supporting Information is available free of charge on the ACS Publications website at DOI: 10.1021/acs.analchem.8b02428.

TEM images, absorption spectra, DLS contributions, inhibitory curves of nanozymes, A/A_0 responses of sensor arrays toward phosphates, additional analysis of hydrolysis reactions catalyzed by apyrase (10:1), and source data about blind samples (PDF)

AUTHOR INFORMATION

Corresponding Author

*E-mail: weihui@nju.edu.cn. Tel.: +86-25-83593272. Fax: +86-25-83594648.

ORCID

Hui Wei: 0000-0003-0870-7142

Author Contributions

§L.Q. and X.W. contributed equally. The manuscript was written through the contributions of all authors. All authors have given approval to the final version of the manuscript.

Notes

The authors declare no competing financial interest.

ACKNOWLEDGMENTS

This work was supported by the National Natural Science Foundation of China (21722503), the 973 Program (2015CB659400), the PAPD Program, the Shuangchuang Program of Jiangsu Province, the Open Funds of the State Key Laboratory of Analytical Chemistry for Life Science (SKLACLS1704), the Open Funds of the State Key Laboratory of Coordination Chemistry (SKLCC1819), the Fundamental Research Funds for the Central Universities (021314380103), and the Thousand Talents Program for Young Researchers.

REFERENCES

(1) Hardie, D. G.; Ross, F. A.; Hawley, S. A. *Nat. Rev. Mol. Cell Biol.* **2012**, *13*, 251−262.

(2) Hargrove, A. E.; Nieto, S.; Zhang, T.; Sessler, J. L.; Anslyn, E. V. *Chem. Rev.* **2011**, *111*, 6603−6782.

(3) Esipenko, N. A.; Koutnik, P.; Minami, T.; Mosca, L.; Lynch, V. M.; Zyryanov, G. V.; Anzenbacher, P. *Chem. Sci.* **2013**, *4*, 3617−3623.

(4) Przedborski, S.; Vila, M. *Clin. Neurosci. Res.* **2001**, *1*, 407−418.

(5) Zheng, D.; Seferos, D. S.; Giljohann, D. A.; Patel, P. C.; Mirkin, C. A. *Nano Lett.* **2009**, *9*, 3258−3261.

(6) Harold, F. M. *Bacteriol. Rev.* **1966**, *30*, 772−794.

(7) Jiang, G.; Zhu, W.; Chen, Q.; Shi, A.; Wu, Y.; Zhang, G.; Li, X.; Li, Y.; Fan, X.; Wang, J. *Analyst* **2017**, *142*, 4388−4392.

(8) Zhang, L.; Wei, H.; Li, J.; Li, T.; Li, D.; Li, Y.; Wang, E. *Biosens. Bioelectron.* **2010**, *25*, 1897−1901.

(9) Yao, Z.; Feng, X.; Hong, W.; Li, C.; Shi, G. *Chem. Commun.* **2009**, 4696−4698.

(10) Minami, T.; Emami, F.; Nishiyabu, R.; Kubo, Y.; Anzenbacher, P. *Chem. Commun.* **2016**, *52*, 7838−7841.

(11) Wang, Y.; He, X.; Wang, K.; Ni, X. *Biosens. Bioelectron.* **2010**, *25*, 2101−2106.

(12) Zuo, X.; Song, S.; Zhang, J.; Pan, D.; Wang, L.; Fan, C. *J. Am. Chem. Soc.* **2007**, *129*, 1042−1043.

(13) Liu, Y.; Perez, L.; Gill, A. D.; Mettry, M.; Li, L.; Wang, Y.; Hooley, R. J.; Zhong, W. *J. Am. Chem. Soc.* **2017**, *139*, 10964−10967.

(14) Askim, J. R.; Mahmoudi, M.; Suslick, K. S. *Chem. Soc. Rev.* **2013**, *42*, 8649−8682.

(15) Hizir, M. S.; Robertson, N. M.; Balcioglu, M.; Alp, E.; Rana, M.; Yigit, M. V. *Chem. Sci.* **2017**, *8*, 5735−5745.

(16) Rana, S.; Le, N. D.; Mout, R.; Saha, K.; Tonga, G. Y.; Bain, R. E.; Miranda, O. R.; Rotello, C. M.; Rotello, V. M. *Nat. Nanotechnol.* **2015**, *10*, 65−69.

(17) Le, N. D. B.; Yesilbag Tonga, G.; Mout, R.; Kim, S. T.; Wille, M. E.; Rana, S.; Dunphy, K. A.; Jerry, D. J.; Yazdani, M.; Ramanathan, R.; Rotello, C. M.; Rotello, V. M. *J. Am. Chem. Soc.* **2017**, *139*, 8008−8012.

(18) Pode, Z.; Peri-Naor, R.; Georgeson, J. M.; Ilani, T.; Kiss, V.; Unger, T.; Markus, B.; Barr, H. M.; Motiei, L.; Margulies, D. *Nat. Nanotechnol.* **2017**, *12*, 1161−1168.

(19) Liu, B.; Liu, J. *ACS Appl. Mater. Interfaces* **2015**, *7*, 24833−24838.

(20) Hatai, J.; Motiei, L.; Margulies, D. *J. Am. Chem. Soc.* **2017**, *139*, 2136−2139.

(21) He, H.; Li, C.; Tian, Y.; Wu, P.; Hou, X. *Anal. Chem.* **2016**, *88*, 5892−5897.

(22) Liu, J.; Li, G.; Yang, X.; Wang, K.; Li, L.; Liu, W.; Shi, X.; Guo, Y. *Anal. Chem.* **2015**, *87*, 876−883.

(23) Sun, S.; Jiang, K.; Qian, S.; Wang, Y.; Lin, H. *Anal. Chem.* **2017**, *89*, 5542−5548.

(24) Gao, L.; Zhuang, J.; Nie, L.; Zhang, J.; Zhang, Y.; Gu, N.; Wang, T.; Feng, J.; Yang, D.; Perrett, S.; Yan, X. *Nat. Nanotechnol.* **2007**, *2*, 577−583.

DOI: 10.1021/acs.analchem.8b02428
Anal. Chem. 2018, 90, 9983−9989

(25) Wei, H.; Wang, E. *Chem. Soc. Rev.* **2013**, *42*, 6060−6093.
(26) Lin, Y.; Ren, J.; Qu, X. *Acc. Chem. Res.* **2014**, *47*, 1097−1105.
(27) Zhang, Z.; Zhang, X.; Liu, B.; Liu, J. *J. Am. Chem. Soc.* **2017**, *139*, 5412−5419.
(28) Zhang, W.; Hu, S.; Yin, J. J.; He, W.; Lu, W.; Ma, M.; Gu, N.; Zhang, Y. *J. Am. Chem. Soc.* **2016**, *138*, 5860−5865.
(29) Xia, X.; Zhang, J.; Lu, N.; Kim, M. J.; Ghale, K.; Xu, Y.; McKenzie, E.; Liu, J.; Ye, H. *ACS Nano* **2015**, *9*, 9994−10004.
(30) Shen, X.; Liu, W.; Gao, X.; Lu, Z.; Wu, X.; Gao, X. *J. Am. Chem. Soc.* **2015**, *137*, 15882−15891.
(31) Liu, B.; Huang, Z.; Liu, J. *Nanoscale* **2016**, *8*, 13562−13567.
(32) Wei, H.; Wang, E. *Anal. Chem.* **2008**, *80*, 2250−2254.
(33) Wang, X.; Hu, Y.; Wei, H. *Inorg. Chem. Front.* **2016**, *3*, 41−60.
(34) Wang, Q.; Zhang, X.; Huang, L.; Zhang, Z.; Dong, S. *Angew. Chem., Int. Ed.* **2017**, *56*, 16082−16085.
(35) Yao, J.; Cheng, Y.; Zhou, M.; Zhao, S.; Lin, S.; Wang, X.; Wu, J.; Li, S.; Wei, H. *Chem. Sci.* **2018**, *9*, 2927−2933.
(36) Cheng, H.; Lin, S.; Muhammad, F.; Lin, Y.-W.; Wei, H. *ACS Sensors* **2016**, *1*, 1336−1343.
(37) Sharma, T. K.; Ramanathan, R.; Weerathunge, P.; Mohammadtaheri, M.; Daima, H. K.; Shukla, R.; Bansal, V. *Chem. Commun.* **2014**, *50*, 15856−15859.
(38) Hu, Y.; Cheng, H.; Zhao, X.; Wu, J.; Muhammad, F.; Lin, S.; He, J.; Zhou, L.; Zhang, C.; Deng, Y.; Wang, P.; Zhou, Z.; Nie, S.; Wei, H. *ACS Nano* **2017**, *11*, 5558−5566.
(39) Gao, L.; Liu, M.; Ma, G.; Wang, Y.; Zhao, L.; Yuan, Q.; Gao, F.; Liu, R.; Zhai, J.; Chai, Z.; Zhao, Y.; Gao, X. *ACS Nano* **2015**, *9*, 10979−10990.
(40) della Sala, F.; Maiti, S.; Bonanni, A.; Scrimin, P.; Prins, L. J. *Angew. Chem.* **2018**, *130*, 1627−1631.
(41) Li, X.; Wen, F.; Creran, B.; Jeong, Y.; Zhang, X.; Rotello, V. M. *Small* **2012**, *8*, 3589−3592.
(42) Wei, X.; Chen, Z.; Tan, L.; Lou, T.; Zhao, Y. *Anal. Chem.* **2017**, *89*, 556−559.
(43) Yuan, Z.; Du, Y.; Tseng, Y.-T.; Peng, M.; Cai, N.; He, Y.; Chang, H.-T.; Yeung, E. S. *Anal. Chem.* **2015**, *87*, 4253−4259.
(44) Wang, Y.; Zhao, M.; Ping, J.; Chen, B.; Cao, X.; Huang, Y.; Tan, C.; Ma, Q.; Wu, S.; Yu, Y.; Lu, Q.; Chen, J.; Zhao, W.; Ying, Y.; Zhang, H. *Adv. Mater.* **2016**, *28*, 4149−4155.
(45) Cheng, H.; Liu, Y.; Hu, Y.; Ding, Y.; Lin, S.; Cao, W.; Wang, Q.; Wu, J.; Muhammad, F.; Zhao, X.; Zhao, D.; Li, Z.; Xing, H.; Wei, H. *Anal. Chem.* **2017**, *89*, 11552−11559.
(46) De Borba, B. M.; Jack, R. F.; Rohrer, J. S.; Wirt, J.; Wang, D. *J. Chromatogr. A* **2014**, *1369*, 131−137.
(47) Asha, K. S.; Bhattacharjee, R.; Mandal, S. *Angew. Chem., Int. Ed.* **2016**, *55*, 11528−11532.
(48) Yang, J.; Dai, Y.; Zhu, X.; Wang, Z.; Li, Y.; Zhuang, Q.; Shi, J.; Gu, J. *J. Mater. Chem. A* **2015**, *3*, 7445−7452.
(49) Yasin, A.; Li, H.; Lu, Z.; Rehman, S. u.; Siddiq, M.; Yang, H. *Soft Matter* **2014**, *10*, 972−977.
(50) Dittmer, J. C.; Lester, R. L. *J. Lipid Res.* **1964**, *5*, 126−127.
(51) Murphy, J.; Riley, J. P. *Anal. Chim. Acta* **1962**, *27*, 31−36.

DOI: 10.1021/acs.analchem.8b02428
Anal. Chem. 2018, 90, 9983−9989